

Calculation of Coulomb-interaction parameters for La_2CuO_4 using a constrained-density-functional approach

Mark S. Hybertsen and Michael Schlüter

AT&T Bell Laboratories, Murray Hill, New Jersey 07974

Niels E. Christensen

Max-Planck-Institut für Festkörperforschung, Postfach 80 06 65, D-7000 Stuttgart 80, Federal Republic of Germany

(Received 27 December 1988)

The constrained-density-functional approach is used to calculate the energy surface as a function of local charge fluctuations in La_2CuO_4 . This energy surface is then mapped onto a self-consistent mean-field solution of the Hubbard model which allows extraction of the Coulomb interaction parameters when combined with one-electron parameters derived from band-structure results. Variations in the local Cu d charge and in-plane O p charge are considered for the prototypical high- T_c parent oxide La_2CuO_4 . To isolate the charge fluctuations, the calculations are done in a supercell of size up to 2×2 in the basal plane. The local density-functional calculations are done using the linear muffin-tin-orbital approach with the atomic sphere approximation. In the Hubbard Hamiltonian, the Cu $d(x^2-y^2)$ and O $p(x,y)$ orbitals are included in the $pd\sigma$ configuration. The one-electron parameters consist of bare on-site energies (ϵ_p, ϵ_d) and first-neighbor hopping from Cu to O (t_{pd}) and from O to O (t_{pp}) while the Coulomb-interaction parameters include on-site (U_d, U_p) and intersite (U_{pd}, U_{pp}) terms. Results of the present calculation indicate that La_2CuO_4 is intermediate between the extreme spin or charge fluctuation regimes. This places strong constraints on the available parameter space for theories of high- T_c superconductivity based on the extended Hubbard model.

I. INTRODUCTION

There is general theoretical agreement that correlations due to the electron-electron interaction play an important role in the properties of the Cu-O high- T_c superconductors and related compounds. This general feature of $3d$ transition-metal oxides is strongly supported in the present case by the antiferromagnetism observed in the insulating parent phases. It is a long-standing challenge to treat these correlations in the case of strong interactions. Considerable current work is based on the Hubbard model either in a one-band version^{1,2} or an extended three-band form.³⁻⁷ It remains to be shown whether and in which region of parameter space this model can exhibit superconductivity, in addition to the usual magnetic properties. It is therefore important to understand what region of parameter space in the Hubbard model is applicable for the present Cu-O class of materials. The purpose of the present paper is to provide a microscopic, parameter-free calculation of the Coulomb-interaction parameters in the extended Hubbard model for the prototypical case of La_2CuO_4 .

The local density-functional approach (LDA) for calculating ground-state properties has been widely successful for a broad range of materials. However, in cases where local correlations are strong, it tends to lose accuracy or breaks down, e.g., in the case of Fe it predicts the wrong ground state.⁸ Structural calculations have recently been done for La_2CuO_4 showing that the usual calculated bulk properties (e.g., lattice constant, internal structural parameters, bulk modulus, phonon frequencies) agree

with experiment to within standard tolerances.⁹ However, the ground state found with the LDA is paramagnetic, i.e., an antiferromagnetic instability is not sustained.^{10,11} If lattice coupling is included, early indications were that a charge-density-wave state would be obtained.^{12,13} This is in contrast to experiment and more recent calculations.⁹

Despite these difficulties, the LDA has been used successfully to calculate the local Coulomb-interaction parameters in many cases where correlation effects are strong, e.g., transition-metal impurities^{14,15} and NiO.¹⁶ The prototypical case is an open d - or f -shell atom in a metallic host. Here one expects the atomic Coulomb integral (U_{bare}) to be screened by the itinerant electrons in the host to yield an effective or renormalized U . The basic approach for obtaining this U is to calculate the change in the total energy as a function of the local occupation in the d or f shell. The curvature of the energy surface gives the effective U . This is an optimally screened U because the itinerant electrons are allowed to respond self-consistently to the change in local charge density which is assumed to be static. Any dynamical effects reduce screening and tend effectively to increase U . One might initially be sceptical of results for U based on the LDA since the ground state in these materials is often given incorrectly, as noted above. However, the energy scale (and hence the scale on which the charge density must be correct) is relatively large for U . On the other hand, the energy scale associated with the magnetic instabilities (some exchange coupling) is 1 to 2 orders of magnitude smaller. It is the latter which is apparently not adequately treated in the LDA. Since the usual structural properties

are given quite well for La_2CuO_4 ,⁹ the overall charge density must be well represented.

One of the unique features of the Cu-O materials is the strong hybridization of the Cu d level with the in-plane O p level. This is an essential feature in the band structure of these materials^{12,17-20} which makes the Cu-O materials quite distinct from the cases studied previously. A number of fundamental questions arise. (1) A partition of the electronic degrees of freedom must be made separating those electrons which must be considered dynamically from those electrons which may be treated as a passive background which screens the Coulomb interaction. In the prototypical case, the band picture showed a narrow band (or impurity level) coupled to a broad, relatively structureless continuum. In the present case, the $pd\sigma$ band is broad in the one-electron theory, suggesting that the Cu d and O p orbitals must be considered on an equal footing. However, this expands the energy scale considerably, which has to be considered. In addition, the O p orbitals have significant coupling among themselves and to other degrees of freedom which contributes to the width of the bands in the one-electron picture. Thus, there is distinct ambiguity surrounding the isolation of a few bands for correlated treatment. From another point of view, one must establish which portion of the band structure is to be isolated as a starting point for a renormalization treatment and for modeling, e.g., the region near the Fermi surface. (2) One can no longer isolate a single local orbital, the occupation of which is constrained independently of the other bands. The strong overlap here is to be contrasted to the narrow-band impurity limit treated previously. This complicates the treatment of the energy surface as a function of what must in some way be defined as a local charge fluctuation. This must be developed in a way that is consistent with the orbitals explicitly treated in the model Hamiltonian. (3) A nontrivial kinetic energy enters into the problem which must be treated explicitly. Because of the large hopping integrals, the energy surface as a function of local charge state contains a kinetic energy contribution so that the curvature of the energy surface is no longer simply U .

In the present work, we have adopted the point of view from the outset that the Cu d and O p orbitals must be treated on an equal footing. Implicit in this choice is that the one-electron Hamiltonian has been suitably reduced (or down folded) in a first step to eliminate any couplings to other degrees of freedom resulting in proper renormalization of the ε_{ij} . However, we note that orbital degrees of freedom not included here may be important. Guo, Langlois, and Goddard²¹ have based their model on the O $p\pi$ orbitals and the model of Weber²² requires inclusion of the Cu $d(z^2 - 3r^2)$ orbital. Here we restrict ourselves to the three-band model because much current work on mechanisms for high-temperature superconductivity are based on it.³⁻⁷ This choice is discussed further in Sec. IV. The interactions and states included in this Hubbard model are illustrated in Fig. 1. The three-band Hubbard model has the following form:³

$$H = \sum_{i,j,\sigma} \varepsilon_{ij} C_{i\sigma}^\dagger C_{j\sigma} + \frac{1}{2} \sum_{i,j,\sigma,\sigma'} U_{ij} C_{i\sigma}^\dagger C_{i\sigma} C_{j\sigma'}^\dagger C_{j\sigma'}, \quad (1)$$

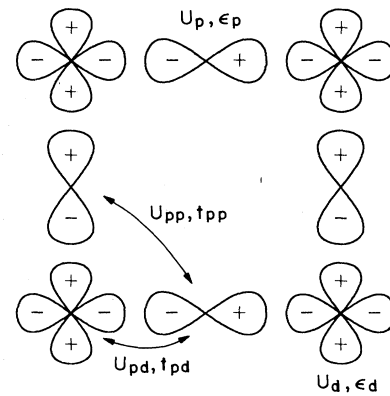


FIG. 1. A schematic presentation of the orbitals and interactions included in the Hubbard model Hamiltonian Eq. (1).

where the ij indices label the planar Cu and O sites, $C_{i\sigma}^\dagger$ creates holes in Cu $d(x^2 - y^2)$ or O $p\sigma(x, y)$ states. The one-electron and Coulomb-interaction parameters, respectively, are the following: on-site ($i=j$) ε_p, U_p and ε_d, U_d ; intersite ($i \neq j$, nearest neighbor) t_{pd}, U_{pd}, t_{pp} , and U_{pp} . As stressed by others,⁷ the direct O-O hopping term t_{pp} is important.

Underlying this model Hamiltonian is some set of appropriate tight-binding orbitals which are assumed to have something like an atomic range. Their exact details are not specified but one should beware that the precise values of the parameters depend on these orbitals. The orbitals used to calculate the parameters must reflect physically sensible choices and be consistent with the application of the model. A related issue is the assumed vacuum state, frequently taken to be Cu^+ and O^{2-} where the d and p shells are fully occupied. Precise values of the parameters also depend on this choice. Finally, the effect of all other electrons not included here are assumed to renormalize (screen) the active parameters.

Two classes of parameters are required for Eq. (1): the one-electron ε_{ij} , and the Coulomb interaction U_{ij} . The one-electron parameters are obtained under the assumption that the LDA bands can be interpreted as corresponding to the mean-field (MF) solutions of Eq. (1), as pointed out by Emery.³ The Coulomb parameters are calculated from the total energy in the constrained-density-functional approach. Of course, these two procedures are coupled. Each depends on the full set of one-electron and Coulomb parameters. A final, unique set of parameters is obtained which is consistent both with the LDA band structure and the constrained-density-functional total-energy results.

The crucial one-electron parameter in the problem is the difference in on-site energies $\varepsilon = \varepsilon_p - \varepsilon_d$. In establishing the parameters in Eq. (1), one must keep in mind that the appropriate ε is "bare." The ε^{MF} from the fit to the LDA band structure is screened. The ε^{MF} is unscreened to obtain ε using a mean-field solution to Eq. (1). This is an approximation which we expect to be appropriate for extended systems such as the present one with strong hopping (covalency). Furthermore, the precise values of the

ε_{ij} generally depend on the portion of the band structure to be reproduced, e.g., the region near the Fermi surface. The reason for this is the coupling of the orbitals in the restricted space spanning Eq. (1) to other degrees of freedom, e.g., the Cu s orbitals. These issues are important for obtaining a consistent set of parameters and are discussed in more detail in the body of the paper.

Since the Coulomb parameters U_{ij} cannot be related directly to a particular narrow band, two developments are introduced in order to treat this more complex situation. We break the problem into two parts. First, the energy surface as a function of local charge state is obtained microscopically using a constrained-density-functional approach. The constraint must be introduced explicitly into the problem in real space since the orbital occupancy cannot be independently controlled. The result of this calculation is a variationally optimized energy surface as a function of appropriate local charge fluctuations. Second, the Hubbard model Eq. (1) is solved explicitly in mean field as a function of local charge state in parallel with the density-functional calculations. The underlying Coulomb-interaction parameters are then extracted as those which give an energy surface matching that from the microscopic density-functional calculation. In this way, the kinetic energy in the present covalent situation is properly handled and the Coulomb-interaction parameters are screened correctly for the appropriate crystalline environment. This approach not only yields the screened Coulomb-interaction parameters from the effective curvatures of the energy surface near the ground state, but it also can indicate secondary metastable states, if such exist, provided these states are connected with the ground state via the charge fluctuations considered. Metastable states have been found, e.g., in magnetic systems when magnetization and volume were constrained.²³ In the present case, we found no indications of any metastability within the space of Cu d and O p charge fluctuations.

$$\begin{aligned}
 E = & \frac{1}{2} \tilde{U}_d [(\delta n_{d1})^2 + 2(\delta n_{d2})^2 + (\delta n_{d3})^2] + \frac{1}{2} \tilde{U}_p [4(\delta n_{p1})^2 + 4(\delta n_{p2})^2] \\
 & + \tilde{U}_{pd} (4\delta n_{d1}\delta n_{p1} + 4\delta n_{d2}\delta n_{p1} + 4\delta n_{d2}\delta n_{p2} + 4\delta n_{d3}\delta n_{p2}) \\
 & + \tilde{U}_{pp} [4(\delta n_{p1})^2 + 4(\delta n_{p2})^2 + 8\delta n_{p1}\delta n_{p2}].
 \end{aligned} \tag{2}$$

Fitting of the calculated points on the energy surface yields the curvatures \tilde{U}_{ij} . These are then matched by the curvatures found in the mean-field solution of Eq. (1) which implicitly determines Coulomb-interaction parameters U_{ij} .

The mapping onto the restricted subspace of Eq. (1) depends on a consistent set of one-electron parameters ε_{ij} of which $\varepsilon = \varepsilon_p - \varepsilon_d$ is the key. The results obtained from the mapping for U_d , U_{pd} , and U_{pp} are insensitive to ε , while U_p is strongly dependent on ε . The final²⁴ numerical results were as follows: $U_d = 10 \pm 1$ eV, $U_p = 3$ to 8 eV depending on ε varying from 4 to 2 eV, $U_{pd} = 1.2 \pm 0.5$ eV, and $U_{pp} \approx 0$. A consistent set of one-electron and Coulomb-interaction parameters are collected in Table I. These are based on a value of $\varepsilon = 3.6$ eV, a choice which is justified in detail in Sec. IV.

For comparison, the parameters appropriate for Eq. (1)

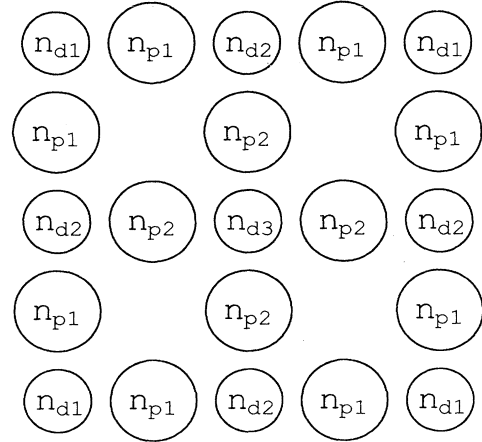


FIG. 2. A schematic presentation of the charge degrees of freedom considered in the 2×2 unit cell and the atoms taken to be equivalent in the basal plane.

Most of the calculations were carried out for a 2×2 supercell indicated schematically in Fig. 2. The charge degrees of freedom considered are shown with the symmetry indicated. In comparison to test calculations on 1×1 and $\sqrt{2} \times \sqrt{2}$ cells, it was found that the screening response to the charge perturbations induced were sufficiently converged with this size cell. This shows that the local charge fluctuations were sufficiently isolated. Various combinations of constraints were considered to ensure that the energy surface was adequately sampled. Local constraints, e.g., on the central Cu(1) site, lead to responses throughout the cell in the channels shown in Fig. 2. In order to form an orderly data set taking into account charge fluctuations in the Cu d and O p channels throughout the 2×2 unit cell, the charge fluctuations were combined according to the following form:

TABLE I. Comparison of the present set of parameters for the extended Hubbard model with the parameters recommended by other authors. Hole notation is adhered to in ordering the energies and the phase conventions according to Fig. 1 are used. The value of U_p depends sensitively on the choice of ε as shown in Fig. 8.

	Present	Ref. 7	Ref. 25
ε^{MF}	1.3	...	1.2
ε	3.6	1.5	...
t_{pd}	1.3	1.07	1.6
t_{pp}	0.65	0.53	0.65
U_d	10.5	9	8.5
U_p	4	6	4.1-7.3
U_{pd}	1.2	1.5	≥ 0.6
U_{pp}	0	1	...

have been estimated by other groups in various ways. Jenison and Stechel⁷ have combined the band-structure results for the one-electron parameters with interpretation of Auger spectra for related oxides and screening estimates to obtain the U_{ij} . The parameters have also been independently calculated by other groups using an approach similar to but different from that employed here.^{11,25,26} A key difference is that the orbitals of interest, e.g., the Cu d , have been artificially isolated by zeroing the relevant Hamiltonian matrix elements coupling that orbital to the others for purposes of varying the orbital occupation to obtain the Coulomb parameters, e.g., U_d . This procedure also provides an alternative approach for obtaining the on-site energy difference ε . This isolation of the relevant orbital reproduces the limit where the strongly correlated electrons (large U) are in a localized (atomic) level with no coupling to a continuum. It is presumably still quite reasonable for the case of finite coupling to a continuum. Our procedure, in contrast, is explicitly designed for the present case of periodic correlated electrons with strong hopping and where the "continuum" is derived in part from the electrons which themselves have important local Coulomb correlations. These differences of approach are described in more detail in Sec. III D. Interestingly, there is general agreement between the parameter sets. Parameters have also been suggested using a cluster-based analysis of experiments and a tight-binding fit to the LDA bands.²⁷

The balance of the present paper is organized as follows. Section II contains a brief description of the constrained-density-functional approach. The details of the application to the La_2CuO_4 system are contained in Sec. III. The results are discussed in Sec. IV, in comparison to other calculations and available experimental data. The various mechanisms for pairing proposed on the basis of the Hubbard model Hamiltonian are analyzed in view of our results.

II. CONSTRAINED-DENSITY-FUNCTIONAL APPROACH

The constrained-density-functional approach has been described in rather general form.¹⁴ Applications have been made to Coulomb-interaction parameters in narrow band¹⁶ or impurity^{14,15} situations as well as to the study of itinerant magnetic systems.²³ Here we outline the elements of the approach required in the present context.

For purposes of developing the approach, the case of local d -charge (N_d) fluctuations is considered. The energy as a function of N_d is required. This is obtained in the density-functional approach by minimizing the total energy subject to the constraint that the local d charge by N_{id} . The value of the local d charge on site i is defined in terms of a projection operator:

$$n_{id}(\mathbf{r}) = \sum_{n,\mathbf{k}}^{\text{occ}} n_{n\mathbf{k}} |(\hat{P}_{id}\phi_{n\mathbf{k}}(\mathbf{r}))|^2. \quad (3)$$

Here the $\phi_{n\mathbf{k}}$ are the Kohn-Sham orbitals in the density-functional approach with occupation $n_{n\mathbf{k}}$. States are indexed in a periodic crystalline system. The required form of the projection operator \hat{P}_{id} depends on the model. In

this case, it must be centered around the relevant Cu site, have some specified range, and perhaps impose a particular shape as well. For example, the projection might be on a specific form of the $d(x^2-y^2)$ orbital. A somewhat general form acting on function $f(\mathbf{r})$ might be

$$(\hat{P}_{id}f)(\mathbf{r}) = \phi_d(\mathbf{r}-\mathbf{R}_i) \int d\mathbf{r}' \phi_d^*(\mathbf{r}'-\mathbf{R}_i) f(\mathbf{r}'), \quad (4)$$

where normalization of the volume integral of $|\phi_d|^2$ to unity ensures that \hat{P}_{id} is idempotent as well as Hermitian. The choice of the radial form of ϕ_d in the present problem should be dictated by the orbitals underlying the Hubbard model Eq. (1).

The total energy of the constrained system can be established variationally,¹⁴ just as in the standard case.²⁸ The relevant energy expression is

$$E(N_{id}) = \min \left[E[n] + \lambda_{id} \left[\int d\mathbf{r} n_{id}(\mathbf{r}) - N_{id} \right] \right], \quad (5)$$

where $E[n]$ is the usual density functional and λ_{id} is a Lagrange multiplier. Upon carrying out the minimization using the usual procedure, there is an additional term in the Kohn-Sham equations (a local impuritylike potential) which enforces the local constraint:

$$(T + V_{\text{ext}} + V_H + V_{\text{xc}} + \lambda_{id}\hat{P}_{id})\phi_{n\mathbf{k}} = \varepsilon_{n\mathbf{k}}\phi_{n\mathbf{k}}. \quad (6)$$

Here the usual terms enter: the kinetic energy, external potential (interaction with the ion cores), the average electrostatic potential (Hartree), and the density-functional exchange-correlation potential. The additional term arises from the constraint and acts to change the value of $n_{id}(\mathbf{r})$. In principle, λ_{id} is varied to satisfy the constraint. In practice, for each λ_{id} a particular N_{id} results and the energy surface $E(N_{id})$ is obtained.

This then is a variational procedure for calculating the energy associated with local charge fluctuations. As such, it produces the optimally screened energy. Also, because it is variational, this procedure yields an energy surface which is quadratic in $N_{id} - N_{id}^0$ to lowest order where N_{id}^0 is the ground-state value (i.e., no constraints).

The procedure described is easily generalized to the case of interest here where both O p charge N_p and Cu d charge N_d are involved. Because we use a one-to-one mapping of the constraint N_{id} and the Lagrange multiplier λ_{id} (assuming that the ground state is stable in the regime of charge fluctuations considered), it is simpler to think of the λ_{id} as a perturbation leading to a particular charge response N_{id} . In order to map the energy surface adequately, perturbations are considered in the Cu d and O p channels both separately and together. Because of the strong covalent overlap, perturbation of a particular central site will lead to charge response in the Cu d and O p channels on neighboring sites as well. Therefore, strictly speaking, the present approach maps out the energy as a functional of charge profiles in these channels. This is treated by assuming that the energy surface near the ground-state configuration can be expanded in terms of the integrated local charge fluctuations on the central site and those nearby, which was illustrated for the Cu-centered 2×2 supercell case in Eq. (2). In this way, the energy surface as a function of many individual charge fluctuations is described compactly in terms of a few pa-

rameters. We refer to this generically as $E(N_p, N_d)$. Equivalently, we also considered O-centered supercells which lead to expressions similar to Eq. (2).

Given the energy surface $E(N_p, N_d)$, the results must be mapped back onto the Hubbard model. In the decoupled impurity limit ($t=0$), this is trivial. The Coulomb parameters are the quadratic terms \tilde{U} in the energy surface expanded with respect to $N_d - N_d^0$ and $N_p - N_p^0$. The present case is in the opposite limit, namely of strong covalent overlap. Because the hopping term is important, the quadratic terms in the energy surface include a substantial kinetic energy contribution. This is a non-negligible effect and is independent of the use of supercells. In order to properly obtain the Hubbard parameters, the energy surface calculated in the constrained-density-functional approach must be compared directly with solutions of the Hubbard model. This is done using a self-consistent mean-field (Hartree-Fock) solution of the Hubbard model which maintains the analogy to the density-functional calculations. Details of the necessary tight-binding calculations are given below in Sec. III C.

III. APPLICATION TO La_2CuO_4

A. LDA calculations

The LDA calculations are carried out using the linearized muffin-tin-orbital (LMTO) approach with the atomic spheres approximation (ASA).²⁹ The basic unit cell is body-centered tetragonal with one formula unit per cell. In addition to spheres around each atomic site, two empty spheres are introduced. The positions and radii of the spheres used are indicated in Table II. Two energy panels are considered. In the lower panel, the La $5s$ and $5p$ bands as well as the O $2p$ bands are treated. The balance of the valence states are treated in the upper panel. The remaining core charge is frozen. The angular momentum components retained in the basis in each sphere are shown in Table II. The Brillouin zone is sampled by 12 special k points in two layers in the irreducible $\frac{1}{16}$ portion of the zone. Our results are essentially unchanged by use of more points or by use of a linear tetrahedron sampling technique. Densities of states presented below were calculated using the latter technique. The correlation data used in the LDA is taken from Ref. 30.

The resulting self-consistent band structure is given in Fig. 3 with the corresponding density of states in Fig. 4. Comparison of these results to full potential linear augmented-plane-wave (LAPW) calculations^{12,17} shows that the important Cu-O bands are well represented. The position of the Fermi level relative to the small van Hove singularity just below is correct. This also agrees with earlier LMTO calculations.³¹ The three notable deviations from the LAPW calculations are (i) the quantitatively incorrect dispersion and placement of the empty La d and f states; (ii) the weight in the occupied density of states is distributed more asymmetrically; (iii) the Cu-O bands are about 1 eV wider. These differences are not expected to have significant impact on the present calculation of the Coulomb-interaction parameters.

TABLE II. Atomic positions, sphere radii (S) and basis functions used for the present LMTO-ASA calculation for La_2CuO_4 . O(1) denotes the planar oxygen, O(2) the apical oxygen, and E an empty sphere. Positions are in units of $a/2$ with $a = 3.79$ Å and $c/a = 3.485$ in the body-centered-tetragonal cell.

	Position			S (Å)	Basis	
	x	y	z		panel 1	panel 2
Cu	0.0	0.0	0.0	1.233	spd	spd
O(1)	1.0	0.0	0.0	1.115	sp	spd
	0.0	1.0	0.0			
O(2)	0.0	0.0	-1.269	1.115	sp	spd
	0.0	0.0	1.269			
La	1.0	1.0	-0.962	1.820	spd	$spdf$
	1.0	1.0	0.962			
E	1.0	0.0	1.7425	1.162	sp	spd
	0.0	1.0	1.7425			

In order to spatially isolate to the extent possible the perturbations used to induce charge fluctuations, supercells are employed. Several cases involving one-, two-, or four-formula units per unit cell were considered, both allowing a single Cu atom or a single planar O atom to be crystallographically inequivalent from the others. The cases considered were 1×1 , $\sqrt{2} \times \sqrt{2}$, and 2×2 , all in the basal plane. Interplanar coupling is not important. In the largest unit cell, the Cu charge fluctuations are separated by about 7.6 Å. The final results are given for a Cu-centered four-formula unit cell which is 2×2 in the basal plane. The symmetry is indicated by Fig. 2 showing three inequivalent Cu sites and two inequivalent O sites in the plane. Screening responses from all atoms in the full unit cell are allowed. The lattice is a special case of the triclinic type with a vertical mirror plane along the diagonal. The parameters of the calculation carry straight over from

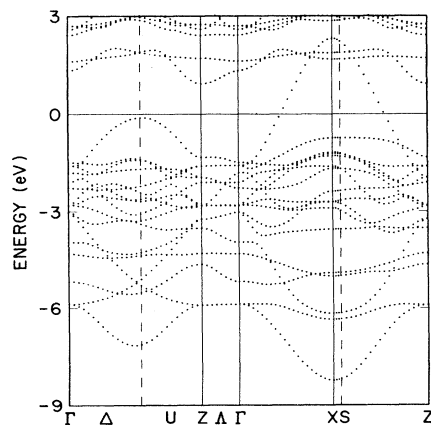


FIG. 3. The LDA energy band structure from the present LMTO-ASA calculation plotted along symmetry lines following Ref. 10. The Fermi energy is the 0 of energy.

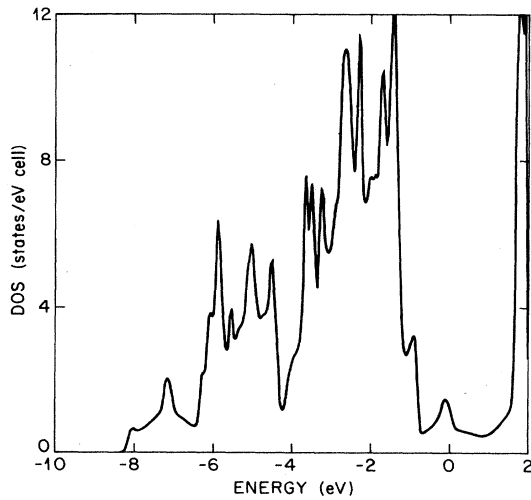


FIG. 4. The LDA density of states from the present LMTO-ASA calculation. Gaussian broadening of 0.1-eV full width at half maximum is included.

the 1×1 cell to the present case with a fourfold increase in the basis set size. The irreducible quarter of the Brillouin zone is sampled by 16 points that result from folding the 12 point set used in the 1×1 body-centered-tetragonal cell back to the present zone. This results in complete compatibility with the calculations in the original unit cell and properly preserves the original symmetry in the absence of perturbations. By basing the final results on a single supercell geometry, numerical “noise” in the total energies is kept to a minimum.

B. Calculation of the energy surface: LDA

The use of the LMTO-ASA approach for the total energy calculations essentially dictates a natural approximation for the projection operator in the constraints. The projector is taken to be simply the angular momentum projector \hat{P}_l inside the relevant atomic sphere and zero outside. This corresponds to evaluating the relevant charge channel as the angular momentum decomposition of the charge in the atomic sphere. Thus, the Cu d charge, for example, is constrained to have a particular value in the Cu atomic sphere. A specific orbital shape is not imposed and the different m orbitals in the d manifold are not distinguished at this stage. The resulting constraint potential in the Kohn-Sham equations is simply a constant for the d electrons inside the Cu atomic sphere and zero otherwise. For the relatively localized Cu $3d$ orbitals, limiting the constraint to the atomic sphere is not too severe an approximation. Most of the atomiclike wave function is inside the sphere. However, the more extended O $2p$ orbitals have significant weight beyond their spheres. Part of the weight that falls in the O p channel in a simplified tight-binding picture is actually represented in the present basis by other angular momentum channels centered on other sites. This complicates the counting of charge in the p channel. Since the projector (and hence

the constraint) are confined to the atomic spheres, two issues must be addressed: (i) does a perturbation that is independent of the quantum number m produce charge fluctuations in channels other than the desired one, e.g., $x^2 - y^2$ for the $l=2$ case; (ii) proper account must be taken of the charge that falls outside the atomic sphere.

The m decomposition of the resulting charge fluctuations δn can be checked. In the case of the Cu d charge, almost 100% falls in the $x^2 - y^2$ channel with a negligibly small portion in the other channels. However, the O p charge is nearly uniformly distributed among x , y (σ and π), and z components. In general, one does not expect the intraorbital Coulomb matrix element to equal the interorbital one. However, this effect can be easily estimated from atomic calculations. For O atoms, the ratio $U_{\text{inter}}/U_{\text{intra}}$ is approximately 0.9. In forming the expression in Eq. (2), this is taken into account by expanding the δn_p into intra- and interorbital components for the on-site terms and introducing the atomic ratio. Note that U_{intra} enters the Hubbard model Eq. (1).

Consistent treatment requires that *all* the relevant charge be taken into account. The final results are being mapped onto the simplified orthogonal tight-binding form given in Eq. (1). By using simplified projectors in the LMTO calculations, the issue of specific atomiclike orbitals has been avoided. Nonetheless, the integrated ground-state charge in the Cu d and especially the O p channels should reproduce the tight-binding result. Of course, N_d and N_p calculated in the LMTO atomic spheres fall short. (Actually, this is a general feature of trying to parse up space and assign angular momentum weights to the charge density.) To overcome this, the LMTO-ASA results are scaled to reproduce the electron count in the tight-binding model (mean field, fit to reproduce the LDA bands in Fig. 3). This is obtained by integrating the occupied portion of the square amplitude in the relevant channel. Then it is assumed that charge fluctuations scale with the total charge. The scale factors employed are 1.033 for N_d and 1.313 for N_p with the choice of atomic sphere radii given in Table II.

The present approach then proceeds with a series of self-consistent LDA total energy calculations for various patterns of imposed perturbations $\{\lambda_i\}$. For each of these, the change in density in the Cu d and O p channels is evaluated as is the effective energy from Eq. (5) yielding points on the energy surface approximated by Eq. (2). The perturbations fall into four distinct classes required to adequately sample the energy surface so that all four parameters in Eq. (2) may be determined. With reference to the 2×2 unit cell and Fig. 2, these are (i) Cu(1) d alone; (ii) O(1) p alone (all four together); (iii) Cu(1) d and O(1) p together and with the same sign; (iv) O(1) p and O(2) p together and with both relative signs. Perturbation of the Cu(1) d channel alone, for example, does lead to some small changes in the other channels. However, this does not give adequate weight to the intersite terms in Eq. (2) which forces the necessity of perturbations in classes (iii) and (iv). In perturbing the O sites, we have chosen to treat all four O(1) sites together. In this way, all the calculations are done in the same unit cell

with the same symmetry and Brillouin-zone sample which minimizes numerical errors.

Typical values of the bare perturbation range up to 0.4 Ry. The on-site response varies up to about 0.3 electrons with the neighboring sites showing a screening response typically a factor of 4 to 8 smaller. As a general rule, the Cu *d* perturbations lead to less neighboring O *p* response than the opposite case. As an example, consider perturbations in class (i), Cu *d* only. For $\lambda=0.4$ Ry, the partial density of states on the perturbed Cu atom is shown in Fig. 5. The repulsive perturbation pushes Cu *d* weight up to and past the Fermi level in comparison to the unperturbed case. The net change in Cu *d* charge is -0.370 electrons. This charge shows up in various channels. The net changes in the central Cu *s* and *p* charges are 0.087 and 0.057 electrons, respectively, showing that due to hybridization, a substantial amount of the screening of the perturbation is on site (about 40%). The redistribution of the partial density of states can be seen in Figs. 5(a) and 5(b). The next most prominent change is on the neighboring Cu(2) atoms (of which there are two; Fig. 2) where the change in *d* electron count is 0.047 per atom and on the planar O(1) atoms (of which there are four) where the change in *p* electron count is 0.020 per atom. The balances of the changes are smaller and spread throughout the other atomic spheres in various angular

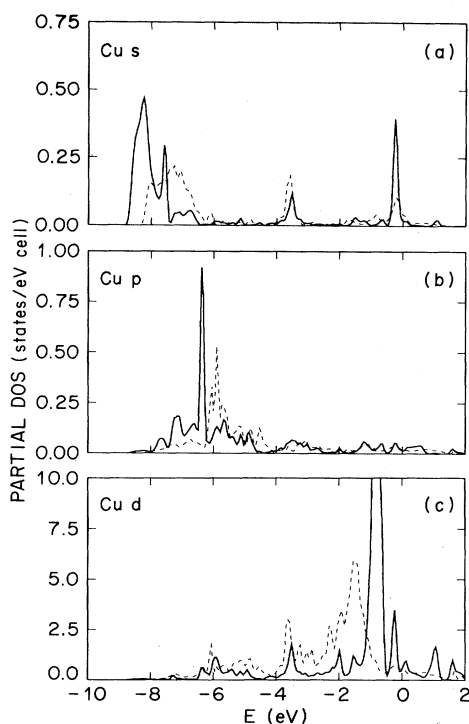


FIG. 5. The partial density of states on the central Cu atom of the 2×2 unit cell in the *s*, *p*, and *d* channels [(a), (b), and (c), respectively] plotted for the unperturbed case (dashed line, integrated values 0.405, 0.451, and 9.242 electrons) and for the case of an $\lambda=0.4$ Ry perturbation in the Cu *d* channel (solid line, integrated values 0.492, 0.508, and 8.872 electrons). Gaussian broadening of 0.1-eV full width at half maximum is included.

momentum channels. When an isolated O atom is perturbed in the *p* channel, a rather different redistribution is observed. For a similar on-site change in *p* charge (-0.326 electrons from $\lambda=0.4$ Ry), there is virtually no on-site screening while the Cu *d* charge changes by about 0.022 electrons per atom and most of the rest of the screening is in the La *d* and *f* channels.

This discussion illustrates the essential complication introduced by the strong covalent overlap in the present system. The local, on-site perturbations lead to a charge response in the channels explicitly treated in the model Hamiltonian Eq. (1) at least on neighboring sites and in some cases further. Clearly, these extended charge responses are characteristic of the couplings and the particular atoms perturbed. It demonstrates the very weak metallic screening exhibited by the present band structure and the importance of local fields in the dielectric screening (microscopic variation in the screening response through the unit cell). One important question is whether the perturbations are sufficiently isolated in the 2×2 unit cell. We have found that the patterns of screening charge around the imposed charge fluctuation from the 2×2 unit cell superpose to yield the separately calculated $\sqrt{2}\times\sqrt{2}$ case rather closely. This suggests that the charge fluctuations are sufficiently separated to allow full screening.

The second point this emphasizes is the importance of using an extended form for fitting the energy surface as shown in Eq. (2). This is illustrated in the following simplified example. Since the O *p* response to the Cu *d* perturbations is rather small, it is reasonable to examine the Cu *d* system in isolation as a first approximation. Even so, there is an extended pattern of *d*-charge response as described above. To account for this, an effective single *d* charge can be defined by

$$(\delta n_{d,\text{eff}})^2 = (\delta n_{d1})^2 + 2(\delta n_{d2})^2 + (\delta n_{d3})^2, \quad (7)$$

and given the sign of δn_{d1} . The calculated effective energy is then fitted to the first term in Eq. (2). The resulting fit is shown in Fig. 6, where a $\tilde{U}_d=13.5$ eV results after renormalization of the *d* charge by the factor of 1.033 not-

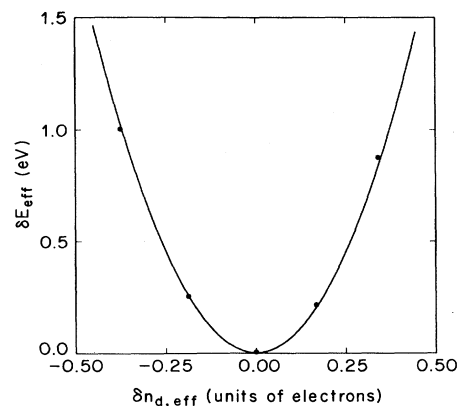


FIG. 6. The effective change in total energy as a function of effective change in Cu *d* charge calculated in the 2×2 cell using the LDA. The solid line is a quadratic fit with no linear term and rms error 0.02 eV.

ed above. (Figure 6 does not include the renormalization.) The quality of the fit is apparent. The slight asymmetry reflects the intersite coupling to the oxygen p channels which was neglected. Note that \tilde{U}_d still contains kinetic energy contributions.

The full data set is fitted by Eq. (2) using a linear least-squares procedure. The result of the fit is $\tilde{U}_d = 13.4$ eV, $\tilde{U}_p = 12.6$ eV, $\tilde{U}_{pd} = 0.1\text{--}0.2$ eV, and $\tilde{U}_{pp} = 0.7$ eV. The rms fitting error is about 0.02–0.05 eV for total energy changes ranging up to about 4 eV depending on the details of the data set used in the final fit. The results of the fit are insensitive to small changes in the data base used. The inclusion of \tilde{U}_{pp} in the fit is important for the final value of \tilde{U}_p because neglect of it would lead to an approximate increase in the apparent value of \tilde{U}_p by $2\tilde{U}_{pp}$. In the next section, we describe the mapping onto a mean-field solution of the Hubbard Hamiltonian. This procedure then allows us to separate in \tilde{U} the Coulomb-interaction parameters U and the kinetic energy contribution.

C. Calculation of the energy surface: Mean-field Hubbard model

We begin with the three-band Hubbard model given in Eq. (1) and apply the usual mean-field approximation (Hartree-Fock) to the interaction terms. This generates mean-field diagonal energies

$$\varepsilon_{d\sigma}^{\text{MF}} = \varepsilon_d + \langle n_{d-\sigma} \rangle U_d + 4U_{pd} \sum_{\sigma'} \langle n_{p\sigma'} \rangle, \quad (8a)$$

$$\varepsilon_{p\sigma}^{\text{MF}} = \varepsilon_p + \langle n_{p-\sigma} \rangle U_p + 2U_{pd} \sum_{\sigma'} \langle n_{d\sigma'} \rangle + 4U_{pp} \sum_{\sigma'} \langle n_{p\sigma'} \rangle, \quad (8b)$$

for the unperturbed, translationally invariant case. For the perturbed case (e.g., 2×2), inequivalent sites are treated separately. The off-diagonal hopping terms t_{pd} and t_{pp} are also renormalized by U_{pd} and U_{pp} , a small effect which we neglect in the present analysis. A self-consistent solution of this Hartree-Fock model, for sufficiently large interactions, yields an antiferromagnetic insulator. As a further approximation, we adopt a spinless formulation ($n_u = n_d = n$) which is compatible with the paramagnetic solution found in LDA. This is essentially a Hartree approximation to the Hubbard model which does not yield the antiferromagnetic ground state. The Hartree approximation modifies the relation between ε and ε^{MF} given above accordingly. We use this for purposes of self-consistent solutions of Eq. (1) in mean field. However, when the bare on-site energies are derived from the band structure ε^{MF} values as discussed in the next section, the Hartree-Fock mean-field solution Eqs. (8) is used together with the mean-field occupation numbers and the Coulomb-interaction parameters.

Now a 12×12 (four unit cells) tight-binding Hamiltonian matrix can be written down. A self-consistent solution is obtained iteratively by integrating in \mathbf{k} space the (hole) states up to the Fermi level, evaluating the individual occupation numbers, and reevaluating the matrix elements. In order to impose charge fluctuations away from the ground state, additional potential terms $\{\lambda_i\}$ are added

to the corresponding diagonal terms in analogy to the constrained-density-functional calculations. The total energy is evaluated by summing over the eigenstates and correcting for the overcounting terms. The energy surface $E^H(N_p, N_d)$ is fitted according to Eq. (2) and effective curvatures \tilde{U}_{ij}^H are obtained. These depend implicitly on all the model parameters ε_{ij} and U_{ij} .

D. Calculated parameters for Hubbard model Hamiltonian

Before the final Coulomb-interaction parameters can be extracted, several issues have to be considered. First consider the kinetic energy contribution to \tilde{U}_{ij}^H . To illustrate this, we plot the quantities \tilde{U}_{ij}^H as a function of the hopping integral t_{pd} ($t_{pp} = 0$) in Fig. 7. The chosen parameters are $U_d = 10.5$ eV, $U_p = 3.5$ eV, $U_{pd} = 1.2$ eV, $U_{pp} = 0.0$ eV, and $\varepsilon = 3.5$ eV. It becomes evident that the effective curvature \tilde{U}_{ij}^H is strongly hybridization dependent. For a covalent system such as La_2CuO_4 ($t_{pd} \approx 1.3$ eV), the kinetic energy contribution can dominate over the Coulomb contribution. This is particularly the case for the O p channel.

Second, the results of the mapping depend on the chosen on-site energy difference, ε . Figure 8 shows that a given set of effective curvatures \tilde{U}_{ij}^H can be obtained by different combinations of U_{ij} and ε . While U_d , U_{pd} , and U_{pp} are relatively insensitive to ε , U_p and ε are strongly interrelated. For instance, for a prechosen $\varepsilon = 2.0$ eV ($\varepsilon^{\text{ME}} \approx 0.0$ eV), the mapping yields $U_p = 8$ eV while for $\varepsilon = 4.0$ eV ($\varepsilon^{\text{ME}} \approx 1.6$ eV), $U_p = 3$ eV. This dependence of the extracted U_p on the choice of ε again reflects the strong influence of hybridization.

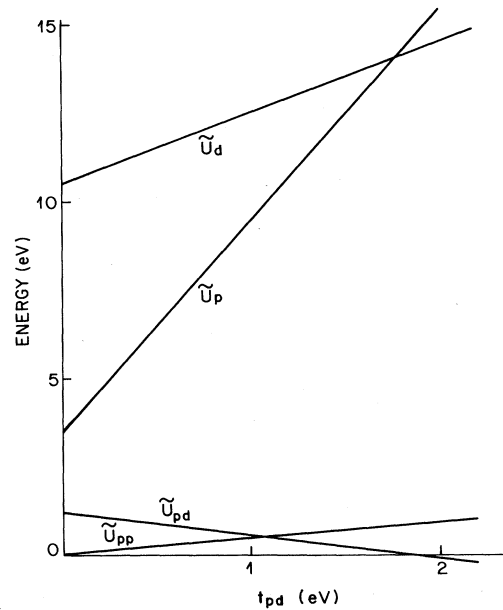


FIG. 7. The dependence of the effective parameters (curvature of the energy surface) on the Cu-O hopping parameter (t_{pd}) as calculated from the self-consistent mean-field solution of the Hubbard model Eq. (1) with the values $\varepsilon = 3.5$ eV, $t_{pp} = 0$, $U_d = 10.5$ eV, $U_p = 3.5$ eV, $U_{pd} = 1.2$ eV, and $U_{pp} = 0$.

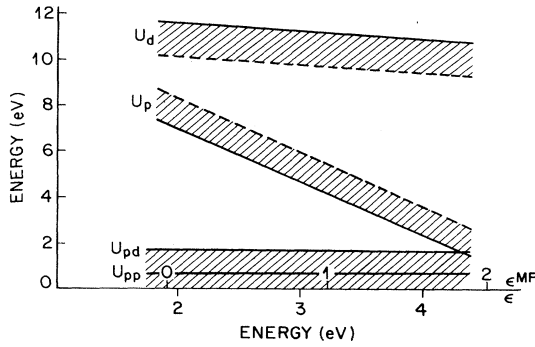


FIG. 8. Final ranges of calculated Coulomb-interaction parameters as a function of the assumed value of the bare on-site energy difference $\epsilon = \epsilon_p - \epsilon_d$ (for holes). The ϵ^{MF} is also shown on a secondary scale.

Finally, the one-electron parameters must be determined. A consistent set of ϵ , t_{pd} , and t_{pp} are required. The crucial parameter that must be established is ϵ , as the other two basically follow from it. As mentioned before, $\epsilon = \epsilon_p - \epsilon_d$ and $\epsilon^{\text{MF}} = \epsilon_p^{\text{MF}} - \epsilon_d^{\text{MF}}$ are the bare and screened on-site (hole) energy differences between the O $p\sigma(x, y)$ and the Cu $d(x^2 - y^2)$ orbitals. One approach adopted here (following Emery³) is to find the screened value from an appropriate tight-binding fit to self-consistent *ab initio* band structure calculations. This was first done by Mattheiss¹² using a minimal orbital set $d(x^2 - y^2)$ and $p\sigma(x, y)$. He pointed out that ϵ^{MF} was small and chose $\epsilon^{\text{MF}} = 0$ for simplicity. It is clear, however, that an equally “good” fit can be obtained for the upper Cu-O band (e.g., in Fig. 3) with ϵ^{MF} ranging from 0 to 2.5 eV by appropriately changing t_{pd} and t_{pp} . In the limited space used in Eq. (1), these parameters cannot be precisely fixed without appealing to quite detailed features of the calculated LDA bands which is not justified given the large central assumption of identifying mean-field solutions of Eq. (1) with the LDA bands in the first place. It is clear that the lower-lying bonding partner of the Cu-O band is significantly coupled to other channels outside the restricted space in Eq. (1). More complete tight-binding fits have been done^{32–34} to the calculated LDA energy bands using either orthogonal or nonorthogonal basis sets. In either case, values of ϵ^{MF} vary from 1.1 to 2.1 eV. One caution regarding this approach is the following. One should now reduce this fit back to the small space spanning Eq. (1). In so doing, the parameters in that space are somewhat re-normalized, a presumably small effect not accounted for here. In any event, it is clear from this discussion that ϵ^{MF} is relatively small, much smaller than for the early transition-metal oxides as has been repeatedly pointed out.³⁵ The final choice of ϵ is dictated by a broader comparison to available data, as discussed below.

As noted in the Introduction, our identification of the LDA bands with the mean-field solution of the Hubbard model Eq. (1) differs from the decoupling approach in Refs. 11 and 25. The latter is modeled after the atomic-like limit where the orbital for the highly correlated electrons is weakly coupled to a metallic continuum (Anderson impurity model). Then the analog of the on-site ener-

gy difference ϵ is the position of the local level relative to the Fermi level. In the limit of no coupling, this is appropriately found from total energy differences between configurations with N and $N - 1$ electrons on the local level, i.e., a discrete removal energy which may also be approximated using a Slater transition state. We point out two important differences between the present three-band Hubbard model for the Cu-O layers in La_2CuO_4 and the model just described. First, the hopping (coupling) is large. Second, the band structure (Fig. 3) shows that the relevant Cu-O bands which are modeled by Eq. (1) and are subject to strong correlation also form an important part of the “continuum” in this system. This is in contrast to the flat localized band weakly coupled to a nearly independent and uncorrelated continuum. We believe that the present situation requires an alternative treatment.

We provide here a brief argument in support of identifying the LDA bands with a mean-field solution of the Hubbard model. This makes clear where the approximation enters in our approach. An orthogonal tight-binding fit to the LDA bands yields in addition to the one-electron parameters, the number of Cu d and O p holes on respective sites. These parametrize the density for a density-functional treatment (DFT) of the Hubbard model Eq. (1). In such a model, the hopping parameters represent the kinetic energy and all the interaction terms are lumped into a single effective potential consisting of the bare external potential and the Hartree plus exchange-correlation potentials. Here this is parametrized by a screened on-site energy difference, $\epsilon^{\text{DFT}} = \epsilon + \epsilon^H + \epsilon^{\text{xc}}$. The variation of the density is achieved solely by varying this ϵ^{DFT} . Then it is clear that the ϵ^{DFT} can be, in principle, exactly obtained by reproducing the density (hole count) in the full microscopic calculation. The problem lies in unscreening ϵ^{DFT} to obtain the bare ϵ . The Hartree potential contribution (ϵ^H) is trivial, but the density-functional exchange-correlation (xc) potential part (ϵ^{xc}) is, in general, unknown. Now the nature of our approximation is clear. We replace the density-functional exchange-correlation potential by the exchange potential calculated from a Hartree-Fock procedure which yields Eqs. (8) where we identify ϵ^{DFT} with ϵ^{MF} (evaluated for paramagnetic spin occupations, following Emery³). This procedure may overestimate the exchange-correlation contribution to the screening of ϵ so that perhaps the actual value should be shifted towards the purely Hartree result (which would increase ϵ somewhat).

The present approach differs from that of Refs. 11 and 25 in the localized limit discussed above. The foregoing discussion shows that this is due to differing approximations for the exchange-correlation part of the screened ϵ^{DFT} . It is important to note that these different approximations make a relatively small difference in the present case. Quantitatively, the procedure of Refs. 11 and 25 gives a value for the bare ϵ which is about 1 eV smaller than that which we find here.

IV. DISCUSSION

Let us return first to the issue of applicability of the LDA to the calculation of Coulomb-interaction param-

ters. We have noted that the LDA clearly fails to describe correctly the ground state of La_2CuO_4 . However, we have argued that this failure occurs on a characteristic energy scale of magnetic interactions which is 1 to 2 orders of magnitude smaller than the characteristic Coulomb energies U . There are many analogous cases, the simplest of which are free-atom Coulomb energies. These can be measured as differences between ionization energies and affinities. The calculations can be done analogously to the present case by varying the occupation of the relevant atomic orbital. For Cu^{2+} , the free ion U derived from $E(d^{10}) + E(d^8) - 2E(d^9)$ is calculated to be 17.1 eV as compared to the experimental value of 16.5 eV. For Cu^+ , the corresponding values are 13.8 and 12.6 eV. These Coulombic energies are well described by our method in contrast to the inability of the LDA to correctly describe the exact ion-multiplet ground states. Applications of the LDA to Coulomb parameters in impurity cases¹⁴ as well as other oxides was also mentioned.¹⁶

We now turn to the discussion of the individual parameters as they are listed in Table I. In hole notation, Weber^{13,32} proposes the values $t_{pd} = 1.4$ eV, $t_{pp} = 0.5$ eV, and $\epsilon^{\text{MF}} = 2.1$ eV using a nonorthogonal orbital set including all the O p , Cu d , and La d orbitals, fit to the LAPW band structure of Mattheiss.¹² The crystal field places the planar oxygen $p\pi$ orbitals lower than the $p\sigma$ orbitals in Eq. (1) by 1.6 eV. An orthogonal fit (to LAPW bands) by Park *et al.*³⁴ yields $t_{pd} = 1.4$ eV, $t_{pp} = 0.6$ eV, and $\epsilon^{\text{MF}} = 1.2$ eV, in quite reasonable agreement with Weber. However, this fit places the planar O $p\pi$ orbitals only about 0.4 eV lower than the $p\sigma$ orbitals. Another orthogonal fit by Papaconstantopoulos, Dewert, and Pickett³³ to LAPW bands gives $t_{pd} = 1.2$ eV, $t_{pp} = 0.1$ eV, and $\epsilon^{\text{MF}} = 1.7$ eV. McMahan, Martin, and Satpathy²⁵ quote $t_{pd} = 1.6$ eV, $t_{pp} = 0.65$ eV, and $\epsilon^{\text{MF}} = 1.2$ eV obtained by fitting to their LMTO band structure through the integrated coupling constants they establish in their impurity Anderson model analysis. Similarly, Zaanen *et al.*¹¹ find $\epsilon^{\text{MF}} \approx 0$ –1 eV. Over all, the hopping parameters are in rough agreement, but the degree of crystal-field splitting allowed as well as the quantitative results for the position of the oxygen $p\pi$ orbitals vary considerably.

We propose the values given in Table I for the one-electron parameters, but caution that mutually compensating variations of the one-electron parameters are possible. The values given in Table I are based on the choice of $\epsilon = 3.6$ eV ($\epsilon^{\text{MF}} = 1.3$ eV). This represents a compromise between a value of ϵ which gives U_p in the experimentally suggested range (discussed below), and a value of ϵ^{MF} which is compatible with the more complete tight-binding fits just described. Then, t_{pd} and t_{pp} follow from a fit to the upper Cu-O band. The resulting t_{pp} is larger than that found by Weber, reflecting the broader Cu-O band in Fig. 3 as compared to the LAPW result.^{12,17} More refined fits to the LDA bands could be possible by including further consideration of the wave-function character or the Fermi surface topology. As noted below, the calculation of the spin-superexchange energy J depends rather critically on values of t_{pd} , t_{pp} , and ϵ , as stressed by Stechel and Jennison.⁷ Thus, J could also be used as a constraint on the choice of one-electron parameters.

The calculated Coulomb parameters are also summarized in Table I. Our value of $U_d = 10.5$ eV is slightly larger than the ones calculated by McMahan, Martin, and Satpathy²⁵ (8.5 eV) and by Chen *et al.*²⁶ (9 eV). Calculations cited by Zaanen *et al.*¹¹ suggest $U_d = 8$ eV. The U values are reduced from the ionic (e.g., Cu^{2+}) value of 16.5 eV due to local dielectric screening. Note that in these other calculations^{11,25,26} the coupling of the Cu d orbital to the O p orbital has been dropped isolating the Cu orbital and allowing the O p states to fully participate in the screening. This probably leads to the smaller estimates for U_d in that work. We note that the O p channel is treated dynamically here in a three-band Hubbard model so it is *not* appropriate to have that extra O p screening renormalize the U_d . Analyses of experiments have also suggested a large Cu U_d . The U_d is inferred from the valence-band satellite seen in resonant-valence-band photoemission which is attributed to a d^8 final state. The value of 6.5 eV is deduced from a simplified analysis by Shen *et al.*³⁶ Also, comparison of core-valence Auger with core and valence x-ray photoelectron spectroscopy (XPS) data allows one to extract the extra energy U_d associated with the localization of two holes on the same Cu site. These data³⁷ suggest U_d in the range 5–7 eV. A simplified calculation of the intra d -shell shake-up process³⁸ suggests that the observed position of the satellite is consistent with $U_d \approx 5$ eV.

The value of $U_p = 4$ eV based on $\epsilon = 3.6$ eV is in reasonable agreement with the results of McMahan, Martin, and Satpathy²⁵ (4–7 eV) but differs significantly from the 14 eV found by Chen *et al.*²⁶ However, the latter is questionable because it is based on incorrectly assumed ionic on-site energies as pointed out by McMahan, Martin, and Satpathy.²⁵ The possibility of finding a sizable U_p associated with oxygen in an ionic material has been questioned on the basis of the small U values (< 1 eV) for *free* O[−] ions. While screening in the solid would indeed reduce this small value further, Madelung-type localization will dramatically increase U . In an ionic solid, the range of O^{2−} or O[−] wave functions is not given by the free ion radius. The constraints imposed by the Madelung-type potentials and orthogonality requirements significantly contract the wave functions which increases U accordingly. In fact, U_p values of order 5 eV, derived from spectroscopy, are typical for oxide materials.³⁹

Relevant to the value of U_p , observation of a direct XPS satellite is reported⁴⁰ which resonates with the O $2s$ absorption threshold and suggests a value of 3–5 eV. The XPS-Auger comparison³⁷ yields a value of $U_p \approx 5$ eV. According to our calculations, this value is possible if $\epsilon \approx 3$ –4 eV or $\epsilon^{\text{MF}} \approx 0.8$ –1.5 eV. Since ϵ is not unambiguously determined from the fitting procedure to the LDA bands, we have used this experimental value of U_p as input to our final choice of ϵ in Table I, as noted above.

The intersite Coulomb energy U_{pd} is calculated by us to be 1.2 eV, in good agreement with the value of ≥ 0.6 eV quoted by McMahan, Martin, and Satpathy.²⁵ Chen *et al.*²⁶ arrive at a higher value of $U_{pd} = 1.6$ eV, but this may be unreliable given the unphysical U_p found in their calculation. A value of order 1 eV for U_{pd} seems rather reasonable to us and is compatible with scaling arguments

as presented by Stechel and Jennison.⁷ Experimentally, a satellite in the Auger spectrum was assigned by Ramaker⁴¹ to the charge-transfer excitation, yielding a value of $U_{pd} \approx 2$ eV. We have also included in our analysis an O-O intersite Coulomb energy U_{pp} . Within error bars, this value was negligibly small.

We turn now to the discussion of various general implications of our results for the electronic parameters of La_2CuO_4 . A satisfactory solution of the multiband Hubbard Hamiltonian Eq. (1) has not been possible to date. Several simplifying approaches have been used. One may neglect the hopping parameters t_{pd} and t_{pp} , at which point the solutions for the disconnected set of atoms becomes trivial. Although La_2CuO_4 is in the opposite limit of large hybridization, the $t=0$ approach yields some useful information in the form of "band centers." In this limit, the ground state of La_2CuO_4 contains one hole per Cu atom, i.e., the configurations are d^9p^6 ($E^n=0$) as follows from the positive ε (for holes). The low-lying (charge) excitation is $d^{10}p^5$ at $E^N=\varepsilon+U_{pd}$, for a hole transferred to a neighboring ligand. If the hole is transferred to a distant ligand site, then the energy is $E^N=\varepsilon+2U_{pd}$. In a photoemission experiment, an extra hole is created and the energies of the various ($N+1$) hole states are d^9p^5 at $E^{N+1}=\varepsilon_p+2U_{pd}$, d^8p^6 at $E^{N+1}=\varepsilon_d+U_d$, $d^{10}p^5p^5$ at $E^{N+1}=2\varepsilon_p-\varepsilon_d+2U_{pd}$, and $d^{10}p^4$ at $E^{N+1}=2\varepsilon_p-\varepsilon_d+U_p+2U_{pd}$. The lowest energy charge excitation decreases from $\varepsilon+U_{pd}$ in the insulator to ε near one oxygen hole or down to $\varepsilon-3U_{pd}$ near three oxygen holes. For the removal of a hole (inverse photoemission), the energy cost is just $E^{N-1}=-\varepsilon_d$. Combined with the E_{N+1} configurations, the possible charge-transfer excitation energies are recovered, depending both on proximity to oxygen holes as well as whether the charge transfer is local (excitonic) or extended.

These simple relations can be used to roughly compare the value adopted here for ε together with the Coulomb parameters to experiments which probe the charge-transfer energy. The simplest case, in principle, is the combined photoemission/inverse photoemission spectrum. The data in Ref. 37 have been interpreted to imply a charge-transfer energy (separated) of 1–2 eV, the separation between the *edges* in the spectrum. If one adopts the $t=0$ limit above, the charge-transfer energy would be just $\varepsilon+2U_{pd}$, taken between "band centers." In this interpretation, one compares to the separation in the peak positions between the spectra, e.g., about 6–7 eV. From our value of U_{pd} , one extracts $\varepsilon \approx 4$ eV. Recognizing that the main photoemission peak includes hybridization with the Cu d electrons, this may be adjusted somewhat to lower ε into the 3–4 eV range. A summary comparison of the present calculated parameters for the Hubbard model to the experimental data is given in Fig. 9. Just as in Ref. 37, photoemission data⁴⁰ is combined with inverse photoemission data.⁴² The predictions of the $t=0$ solution to the Hubbard model are also indicated together with the interpretation of each peak. On the photoemission side, the main feature *B* is emission out of the ligand band ($p^6 \rightarrow p^5$), feature *C* is a satellite that has been established to be O derived involving two holes on an O site (a feature sometimes claimed to be surface sensitive),

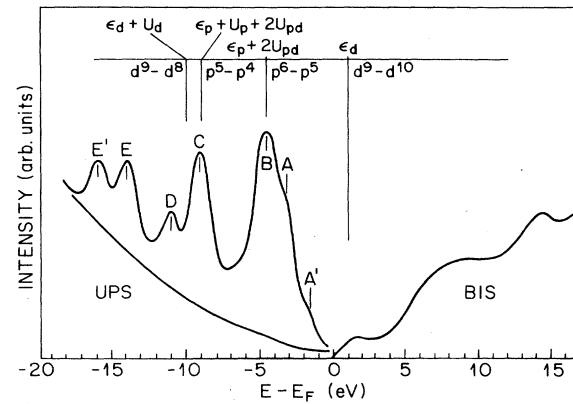


FIG. 9. The photoemission data of Thiry *et al.* (Ref. 40) and inverse photoemission data (BIS) of Royer *et al.* (Ref. 42) are combined on the same scale. For comparison, the "band center" predictions of the Hubbard model with $t=0$ using the present calculated parameters (Table I) are shown.

feature *D* is a Cu-derived satellite involving two holes on a Cu site and features *E* and *E'* are Ba derived and of no interest here. The low-energy bremsstrahlung isochromat spectroscopy (BIS) peak is interpreted as adding an electron to a Cu site ($d^9 \rightarrow d^{10}$). The energies are assigned in the $t=0$ limit as described above yielding the relative positions of these band centers. (The absolute position is adjusted.) As can be seen, the charge-transfer gap, the difference between the $p^6 \rightarrow p^5$ photoemission peak and the $d^9 \rightarrow d^{10}$ BIS peak, agrees very well with our value for $\varepsilon+U_{pd}$. The positions of the satellites is also in good agreement with the calculated values of U_p and U_d , respectively. The $t=0$ analysis is clearly oversimplified. Nonetheless, the agreement seen in Fig. 9 lends support to our calculated parameters given in Table I. Figure 9 also illustrates that La_2CuO_4 is a charge-transfer insulator, but weakly so because the large hopping integrals broaden the bands significantly. As noted above, the separation between the band edges is only 1–2 eV.

The optical absorption^{41,43} and reflectivity³⁷ experiments show structure near 2 eV and a strong edge near 4 eV. With this value of ε , the strong rise in absorption above 4 eV would be due to charge-transfer excitations. However, the latter may also be due to transitions involving cation states, e.g., on the La or Ba sites.⁴³ The charge-transfer interpretation has been adopted by Mila²⁷ and by Geserichs *et al.*⁴⁴ This then leaves the lower-intensity structures near 2 eV a bit open. Geserichs *et al.* identify these with intra-atomic Cu d transitions. Alternatively, these may be excitonic charge-transfer transitions (lowered by U_{pd} in this simple $t=0$ picture). Clearly, hybridization plays an important role in the interpretation of these experiments, but the value of $\varepsilon \approx 3$ eV appears to be consistent.

The question of the deposition of extra holes due to doping may also be addressed initially in the $t=0$ limit. Because of the large size of U_d as compared to ε , the holes will be of predominantly oxygen character. Further refinement would amount to the inspection of the crystal-field splitting obtained from the band-structure fits.

When one does so, it is evident that the $p\pi$ configuration of oxygen $p(x,y)$ orbitals is favored in keeping with the results of more complete calculations by Guo, Langlois, and Goddard.²¹ This is, however, not terribly meaningful at this level since the splittings are small or comparable to the kinetic energy (hopping energies). More detailed calculations are required to address the precise orbital occupied by the extra holes.

More physical insight can be gained from considering small finite clusters (with open or periodic boundary conditions). Many such studies have been undertaken. A rather extensive discussion is given by Stechel and Jennison.⁷ In particular, the Cu-Cu super-exchange J can be computed in this way. We stress that because of the large values of the hopping matrix elements t_{pd} and t_{pp} , the fourth-order (in t) formulas frequently given in the literature are inadequate. Direct calculations are required. Furthermore, because of the strong hybridization, results converge slowly with cluster size. Calculations on three and nine atom clusters⁷ yield J values in the 100-meV range which is compatible with the two-magnon light scattering experiments.⁴⁵ These results depend rather sensitively on the chosen parameters, notably t_{pd} , which was taken as 1.1 eV in Ref. 7. Subsequently, cluster calculations have been done⁴⁶ using the parameters from Table I. These yield $J = 130 \pm 10$ meV in excellent agreement with experiment.⁴⁵ This result confirms the present calculated parameters and in particular, the choice of ϵ . Further cluster calculations⁴⁶ show that parameters based on a smaller value of ϵ , e.g., of order 2 eV, show a slightly reduced value of J . However, parameters based on larger values of ϵ yield values of J that are much too small.

The quantum chemical calculations by Guo, Langlois, and Goddard²¹ for clusters containing just two Cu atoms gave a superexchange energy about a factor of 3 to 4 smaller than experiment. Furthermore, they concluded that the lowest-energy state with an extra hole placed the hole in the $p\pi$ orbitals on the oxygen. Subsequent calculations by Stechel and Jennison⁴⁷ for a Hubbard Hamiltonian, extended beyond Eq. (1) to include the $p\pi$ orbitals, showed that the $p\pi$ orbital is preferred by the extra hole only in the smallest cluster investigated. When clusters with a more realistic number of atoms are considered, the hole has its weight in the $p\sigma$ orbitals on the oxygen atoms, provided the on-site crystal-field splitting between the σ and π orbitals remains smaller than about 1.8 eV. We note that the $p\pi$ orbitals may still play an important role in excitation processes.

Cluster calculations have also been used to further investigate the nature of the quasiparticles introduced by doping. Zhang and Rice² first suggested the formation of a local singlet between the localized hole on the Cu and the dopant hole spread over the four nearest oxygen neighbors in the $p\sigma$ orbitals. Later, McMahan, Martin, and Satpathy²⁵ and Eskes and Sawatzky⁴⁸ confirmed the singlet as the lowest-energy quasiparticle state. The contrary conclusion of Guo, Langlois, and Goddard²¹ connected with the occupation of the $p\pi$ orbitals is probably due to the restricted cluster size and severe underestimates of the superexchange energy. A somewhat different picture is proposed by Stechel and Jennison who introduce

a spin hybrid with varying degree of spin compensation.⁷ It is worth noting that their picture depends crucially on the presence of direct oxygen-oxygen hopping t_{pp} . Other than considering small clusters, the Hubbard Hamiltonian can be approximated as an Anderson impurity Hamiltonian which amounts to keeping U_d but neglecting U_p and U_{pd} as well as any indirect Cu-Cu interactions. This has been done by McMahan, Martin, and Satpathy²⁵ and by Eskes and Sawatzky⁴⁸ to explain photoemission spectra and to investigate the stability of the singlet nature of the quasiparticles as a function of ϵ and U_d . These results also appear compatible with the parameters given here.

We conclude this section with a brief discussion of the implications of our calculated electronic parameters on a variety of pairing models that have been proposed to account for high-temperature superconductivity in the Cu-oxide systems. Emery, in his early pairing model due to the magnetic fluctuations,³ was the first to invoke (hole) carriers localized on the oxygen atoms. This has subsequently been verified^{36,40,49} and agrees with our findings. In his picture the pairing is mediated by a fourth-order double-exchange mechanism resulting in an interaction parameter of order 1 eV when evaluated with our parameters according to his Eq. (4). This is of the right order of magnitude to arrive at high transition temperature (T_c) values when used in a BCS-type theory. Direct oxygen-oxygen hopping (t_{pp}) was not included. A similar BCS-type pairing model between "spin-hybrid" quasiparticles has been proposed by Stechel and Jennison⁷ based on a parameter set in general agreement with our calculations.

Pairing interactions of holes localized in small clusters have been studied numerically by various authors. Ogata and Shiba⁵⁰ consider the extended Hubbard model of Eq. (1) assuming $U_d > \epsilon$ and $t_{pp}, U_p, U_{pd} = 0$. They also assume ϵ large which reduces Cu-O charge fluctuations. Their chosen parameters allow them to transform Eq. (1) into a new effective Hamiltonian (plus correction terms). Using this Hamiltonian, they study clusters with sizes up to 30 atoms. By direct diagonalization it was found that each dopant hole indeed introduced local spin distortions in the underlying antiferromagnetic background. Pairing of two holes can then occur so as to minimize the extent of this spin distortion. An attractive interaction between holes was found for $\epsilon < 3.5t_{pd}$ and U_d large, within the range of parameters in Table I. However, note that t_{pp} and U_{pd} were set to zero. This is in contrast to investigations by Hirsch *et al.*⁶ who considered clusters of up to 16 atoms with the full original Hamiltonian of Eq. (1). From direct diagonalization, they found that the spin-mediated pairing phase, suggested by Ogata and Shiba⁵⁰ is sensitive to finite values of t_{pp} , U_p , and U_{pd} . Similar conclusions were reached by Balseiro *et al.*⁵¹ and by Schüttler and Fedro.⁵² Based on an earlier proposal by Varma *et al.*,⁴ Hirsch *et al.*⁶ suggest a charge-driven pairing phase which requires a small ϵ for access to $d^{10}p^5$ configurations and a relatively large U_{pd} . In particular, for $\epsilon = 1.5$ eV, $t_{pp} = 0$, $U_d = 10$ eV, and $U_p = 3$ eV, Hirsch *et al.*⁶ find that U_{pd} has to be of order 3–4 eV to stabilize a pair of holes in comparison to two separated holes. A smaller value of U_p would be favorable, but according to our calculations, this should be coupled to a larger ϵ which would again be un-

favorable. Furthermore, Hirsch *et al.* show that a finite value of t_{pp} is detrimental to pairing of dopant holes. It seems that all small cluster simulations which have explicitly claimed either spin-driven or charge-driven pairing require electronic parameters which lie outside the intermediate regime calculated here. There is, however, the possibility that these cluster calculations are adversely affected by finite-size effects. On the other hand, possibly a mechanism dependent on both the charge and spin degrees of freedom can be realized within the range of material parameters proposed in this paper. Also, excitations involving other orbital degrees of freedom may play an important role. It should be kept in mind that all these strong-coupling arguments only address the question of an attractive interaction between holes. Superconductivity does not automatically follow. The subtle interplay between the proposed attractive interactions and the kinetic energy of the holes distinguishes the superconductive phase from other charge or spin-ordered phases.⁵³

A different pairing mechanism, driven by intrasite Cu d charge fluctuations has been proposed by Weber.²² In this model, U_d and ε are large and hole conduction occurs only via the direct oxygen overlap t_{pp} . The coupling to an excitonic intrasite Cu $d(x^2 - y^2) \rightarrow d(z^2 - r^2)$ excitation is the mediating interaction in the pairing. Weber bases his model on optical data in which he interprets the observed structures⁴⁴ in the 0.5–2 eV range as due to intrasite Cu crystal-field transitions. He places the charge-transfer excitations at higher energy. These values are roughly consistent with the band-structure crystal-field splittings and our choice of a large ε . The latter would be coupled with an intermediate to small U_p in our parameters. While the Cu d transitions set the energy scale, the coupling between pairs arises from the difference ΔU_{pd} in intersite Coulomb energies between an oxygen hole and either a $d(x^2 - y^2)$ or a $d(3z^2 - r^2)$ hole. This difference has been estimated to be of order 0.5 eV by Weber. This is compatible with our calculations in general terms although outside the restricted subspace considered here. More analysis of the Weber model within the weak-coupling BCS framework has been done by Jarrell, Krishnamurthy, and Cox⁵⁴ who point out some crucial requirements in the interpretation of the low-energy optical data

on which the model hinges.

As a final note, there is the question of whether a one-band Hubbard model is adequate to describe the extra holes introduced in the doped Cu-O layers. Our parameters bear on this question only in so far as such a one-band model is derived from Eq. (1). Otherwise, the parameters entering such a model may reflect a completely different renormalization. Zhang and Rice² have argued in favor of an effective one-band Hubbard model for the dopant-derived holes starting from a version of the three-band Hubbard model Eq. (1). Using our parameters, the singlet level associated with a local Cu d hole bound to an oxygen p hole spread over four neighbors is split off by about 2 eV relative to the nonbonding p -hole combination. As pointed out by Zhang and Rice, this is relatively large compared to an effective hopping energy for the singlet when direct oxygen-oxygen hopping is neglected. Depending on the sign of the t_{pp} , the oxygen-oxygen hopping may destroy the singlet formation.⁵² For the values fitted to the band structure here, we find that the initial splitting of the singlet from the nonbonding p -hole is enhanced, but one must also take into account the itinerant character of the oxygen hole introduced by direct oxygen-oxygen hopping.

In conclusion, we have presented a complete set of electronic parameters for the extended Hubbard model Eq. (1) for the description of the Cu-O planes in the Cu-oxide materials. The results place La_2CuO_4 in the intermediate range between the extreme spin-fluctuation regime and the opposite extreme charge-fluctuation regime. This severely restricts the range of parameter space for theories of quasiparticles, optical excitations, and possible pairing mechanism based on the extended three-band Hubbard model. It may be necessary to expand the subspace in the model to achieve a viable representation of the important physical processes in these materials.

ACKNOWLEDGMENTS

We thank Dr. D. Papaconstantopoulos and Professor W. Weber for sending us their unpublished tight-binding fits.

¹P. W. Anderson, G. Baskaran, Z. Zou, and T. Hsu, *Phys. Rev. Lett.* **58**, 2790 (1987).

²F. C. Zhang and T. M. Rice, *Phys. Rev. B* **37**, 3759 (1988).

³V. J. Emery, *Phys. Rev. Lett.* **58**, 2794 (1987).

⁴C. M. Varma, S. Schmitt-Rink, and E. Abrahams, *Solid State Commun.* **62**, 681 (1987).

⁵J. E. Hirsch, *Phys. Rev. Lett.* **59**, 228 (1987); L. M. Roth, *ibid.* **60**, 379 (1988); J. E. Hirsch, *ibid.* **60**, 380 (1988).

⁶J. E. Hirsch, S. Tang, E. Loh, Jr., and D. J. Scalapino, *Phys. Rev. Lett.* **60**, 1668 (1988); *Phys. Rev. B* **39**, 243 (1989).

⁷E. B. Stechel and D. R. Jennison, *Phys. Rev. B* **38**, 4632 (1988).

⁸C. S. Wang, B. M. Klein, and H. Krakauer, *Phys. Rev. Lett.* **54**, 1852 (1985).

⁹R. E. Cohen, W. E. Pickett, and H. Krakauer, in *Atomic Scale Calculations in Materials Science*, edited by J. Tersoff, D.

Vanderbilt, and V. Vitek (Materials Research Society, Pittsburgh, in press).

¹⁰T. C. Leung, X.-W. Weber, and B. N. Harmon, *Phys. Rev. B* **37**, 384 (1988); P. A. Sterne and C. S. Wang, *ibid.* **37**, 7472 (1988).

¹¹J. Zaanen, O. Jepsen, O. Gunnarsson, A. T. Paxton, and O. K. Andersen, *Physica C* **153-155**, 1636 (1988).

¹²L. F. Mattheiss, *Phys. Rev. Lett.* **58**, 1028 (1987).

¹³W. Weber, *Phys. Rev. Lett.* **58**, 1371 (1987); **58**, 2154(E) (1987).

¹⁴P. H. Dederichs, S. Blugel, R. Zeller, and H. Akai, *Phys. Rev. Lett.* **53**, 2512 (1984).

¹⁵O. Gunnarsson, O. K. Andersen, O. Jepsen, and J. Zaanen, in *Core Level Spectroscopy in Condensed Systems*, edited by J. Kanamori and A. Kotani (Springer-Verlag, Berlin, 1988), p. 82; *Phys. Rev. B* **39**, 1708 (1989).

- ¹⁶M. R. Norman and A. J. Freeman, *Phys. Rev. B* **33**, 8896 (1986).
- ¹⁷J. Yu, A. J. Freeman, and J.-H. Xu, *Phys. Rev. Lett.* **58**, 1035 (1987).
- ¹⁸L. F. Mattheiss and D. R. Hamann, *Solid State Commun.* **63**, 395 (1987); S. Massidda, J. Yu, and A. J. Freeman, *Phys. Lett. A* **122**, 198 (1987), for the $\text{Ba}_2\text{YCu}_3\text{O}_7$ system.
- ¹⁹M. S. Hybertsen and L. F. Mattheiss, *Phys. Rev. Lett.* **60**, 1661 (1988); H. Krakauer and W. E. Pickett, *ibid.* **60**, 1665 (1988); S. Massidda, J. Yu, and A. J. Freeman, *Physica C* **152**, 251 (1988); L. F. Mattheiss and D. R. Hamann, *Phys. Rev. B* **38**, 5012 (1988), for the $\text{Bi}_2\text{Sr}_2\text{CaCu}_2\text{O}_8$ system.
- ²⁰D. R. Hamann and L. F. Mattheiss, *Phys. Rev. B* **38**, 5138 (1988); J. Yu, S. Massidda, and A. J. Freeman, *Physica C* **152**, 273 (1988), for the $\text{Ba}_2\text{Tl}_2\text{Ca}_{n-1}\text{Cu}_n\text{O}_{6+2n}$ system.
- ²¹Y. Guo, J.-M. Langlois, and W. A. Goddard III, *Science* **239**, 896 (1988).
- ²²W. Weber, *Z. Phys. B* **70**, 323 (1988).
- ²³V. L. Moruzzi, P. M. Marcus, K. Schwarz, and P. Mohn, *Phys. Rev. B* **34**, 1784 (1986).
- ²⁴Preliminary results of the present work appeared in M. Schlüter, M. S. Hybertsen, and N. E. Christensen, *Physica C* **153-155**, 1217 (1988).
- ²⁵A. K. McMahan, R. M. Martin, and S. Satpathy, *Phys. Rev. B* **38**, 6650 (1989).
- ²⁶C. F. Chen, X. W. Wang, T. C. Leung, and B. N. Harmon (unpublished).
- ²⁷F. Mila, *Phys. Rev. B* **38**, 11358 (1988).
- ²⁸P. Hohenberg and W. Kohn, *Phys. Rev.* **136**, B864 (1964); W. Kohn and L. J. Sham, *ibid.* **140**, A1133 (1965).
- ²⁹O. K. Andersen, *Phys. Rev. B* **12**, 3060 (1975); H. L. Skriver, *The LMTO Method* (Springer-Verlag, New York, 1984).
- ³⁰U. von Barth and L. Hedin, *J. Phys. C* **5**, 1629 (1972).
- ³¹W. M. Temmerman, G. M. Stocks, P. J. Durham, and P. A. Sterne, *J. Phys. F* **17**, L135 (1987).
- ³²W. Weber (unpublished).
- ³³D. A. Papaconstantopoulos, M. J. Deweert, and W. E. Pickett, in *High Temperature Superconductors*, edited by M. B. Brodsky, R. C. Dynes, K. Kitazawa, and H. L. Tuller, Materials Research Society Symposia Proceedings, Vol. 99 (Materials Research Society, Pittsburgh, 1988), p. 447; and (private communication).
- ³⁴K. T. Park, K. Terakura, T. Oguchi, A. Yanase, and M. Ikeda, Institute for Solid State Physics, Tokyo University, Tokyo, Japan, Technical Report No. 1960, Ser. A, 1988 (unpublished).
- ³⁵J. A. Wilson, *J. Phys. C* **20**, L911 (1987).
- ³⁶Z.-X. Shen *et al.*, *Phys. Rev. B* **36**, 8414 (1987).
- ³⁷D. van der Marel, J. van Elp, G. A. Sawatzky, and D. Heitmann, *Phys. Rev. B* **37**, 5136 (1988).
- ³⁸K. J. Chang, M. L. Cohen, and D. R. Penn, *Phys. Rev. B* **38**, 8691 (1988).
- ³⁹G. A. Sawatzky and D. Post, *Phys. Rev. B* **20**, 1546 (1979).
- ⁴⁰P. Thiry, G. Rossi, Y. Petroff, A. Revcolevschi, and J. Jegoudez, *Europhys. Lett.* **5**, 55 (1988).
- ⁴¹D. E. Ramaker, in *Chemistry of High Temperature Superconductors II*, edited by D. L. Nelson and T. F. George (American Chemical Society, Washington, DC, 1988), p. 84.
- ⁴²W. A. Royer, R. J. Cava, and N. V. Smith (unpublished).
- ⁴³S. Etemad, D. E. Aspnes, M. K. Kelly, R. Thompson, J. M. Tarascon, and G. W. Hull, *Phys. Rev. B* **37**, 3396 (1988).
- ⁴⁴H. P. Gesserichs, G. Scheiber, J. Geerk, H. C. Li, G. Linker, W. Assmus, and W. Weber, *Europhys. Lett.* **6**, 277 (1988).
- ⁴⁵K. B. Lyons, P. A. Fleury, J. P. Remeika, and T. J. Negran, *Phys. Rev. B* **37**, 2353 (1988); K. B. Lyons, P. A. Fleury, L. F. Schneemeyer, and J. V. Waszczak, *Phys. Rev. Lett.* **60**, 732 (1988).
- ⁴⁶E. B. Stechel (private communication).
- ⁴⁷E. B. Stechel and D. R. Jennison, *Phys. Rev. B* **38**, 8873 (1988).
- ⁴⁸H. Eskes and G. A. Sawatzky, *Phys. Rev. Lett.* **61**, 1415 (1988).
- ⁴⁹J. M. Tranquada *et al.*, *Phys. Rev. B* **36**, 5263 (1987); N. Nucker *et al.*, *ibid.* **37**, 5158 (1988).
- ⁵⁰M. Ogata and H. Shiba (unpublished).
- ⁵¹C. A. Balseiro, A. G. Rojo, E. R. Gagliano, and Y. B. Alascio (unpublished).
- ⁵²H. B. Schüttler, *Phys. Rev. B* **38**, 2854 (1988); H. B. Schüttler and A. J. Fedro (unpublished).
- ⁵³S. Robaszkiewicz, R. Micnas, and K. A. Chao, *Phys. Rev. B* **23**, 1447 (1981).
- ⁵⁴M. Jarrell, H. R. Krishnamurthy, and D. L. Cox, *Phys. Rev. B* **38**, 4584 (1988).